electronics

MDPI

Article

Luminescent Downshifting Silicon Quantum Dots for Performance Enhancement of Polycrystalline Silicon Solar Cells

Qais Masaadeh [1], Eleni Kaplani [1,*] and Yimin Chao [2]

[1] School of Engineering, Faculty of Science, University of East Anglia, Norwich Research Park, Norwich NR4 7TJ, UK
[2] School of Chemistry, Faculty of Science, University of East Anglia, Norwich Research Park, Norwich NR4 7TJ, UK
* Correspondence: e.kaplani@uea.ac.uk

Abstract: Silicon quantum dots (Si-QDs) with luminescent downshifting properties have been used for the efficiency enhancement of solar cells. In this study, Phenylacetylene-capped silicon quantum dots (PA Si-QDs) have been fabricated and applied as luminescent downshifting material on polycrystalline silicon solar cells, by dropcasting. The PA Si-QD coated solar cell samples presented an average increase in the short circuit current (Isc) of 0.75% and 1.06% for depositions of 0.15 mg and 0.01 mg on 39 mm × 39 mm pc-Si solar cells, respectively. The increase was further enhanced by full encapsulation of the sample leading to overall improved performance of about 3.4% in terms of Isc and 4.1% in terms of power output (Pm) when compared to the performance of fully encapsulated reference samples. The PA Si-QD coating achieved a reduction in specular reflectance at 377 nm of 61.8%, and in diffuse reflectance of 44.4%. The increase observed in the Isc and Pm is a promising indicator for the use of PA Si-QDs as luminescent downshifting material to improve the power conversion efficiency of pc-Si solar cells.

Keywords: luminescent downshifting; pc-Si solar cells; phenylacetylene; silicon quantum dots

Citation: Masaadeh, Q.; Kaplani, E.; Chao, Y. Luminescent Downshifting Silicon Quantum Dots for Performance Enhancement of Polycrystalline Silicon Solar Cells. *Electronics* **2022**, *11*, 2433. https://doi.org/10.3390/electronics11152433

Academic Editors: Elias Stathatos, Emmanuel Kymakis and Dimitris A. Chalkias

Received: 2 May 2022
Accepted: 1 August 2022
Published: 4 August 2022

1. Introduction

Solar cell efficiencies are continuously updated with new generation solar cells reaching improved efficiencies [1]. However, there is a constant effort in exploring solutions for improving further the efficiency of the mature technology of crystalline silicon cells. Crystalline silicon solar cells, sc-Si, and pc-Si exhibit high EQEs in the visible/near-infrared (NIR) region (430–1000 nm) of the incident solar radiation [2,3]. Their spectral response peaks between 850 and 950 nm at >95%, while it is reduced between 20–55% in the range of 300–500 nm [4]. With the largest portion of spectral irradiance ranging between 300–700 nm (at sea level AM1.5), it is bound to lose 149 W/m^2 of the incident 1000 W/m^2; for reference, the usable fraction of the solar spectrum by Si solar cells amounts to less than half at 468 W/m^2 [5].

Advanced solutions including the use of additives such as luminophores, and solar converters, such as dyes, luminescent downshifting (LDS), and upshifting devices have been proposed, including the application of quantum dots (QDs), and luminescent solar concentrators, to better match the spectral response of pc-Si solar cells to that of the solar spectrum [6]. LDS involves the conversion of one high-energy photon into a lower-energy one where the spectral response of the solar cell is higher and can be more efficiently absorbed by the solar cell. LDS is considered a subcategory of the quantum process called down-conversion (DC). The first attempt in exploring the use of DC to split a high-energy UV photon into two visible light photons was carried out by Dexter in 1957 [7]. DC can be achieved by the use of host materials (lattices or ions) to achieve quantum efficiencies (QE) bigger than unity [8], as discussed, demonstrated, and modelled by researchers in the literature [9–13]. The difference between DC and LDS is the QE achieved by either process;

in LDS, a high-energy photon is cut down to a singular low-energy photon and losses due to thermalisation [14], and thus QE below unity. One of the earliest uses of LDS materials to improve solar cells was performed by Hovel et al. in 1979 [15], where plastic fluorescent materials were implemented for cells with sharp cut-offs in spectral response, and ruby for cells with more gradual cut-offs; efficiency improvements were measured at 0.5–2%. Several different approaches have been used to introduce LDS material to solar cells, with the general trend being adding a transparent host layer that houses the LDS materials on top of the cells. The most used materials were polymethylmethacrylate (PMMA), clear glass, and ideal plastics. These hosted LDS materials such as organic dyes, QDs, and organometallic complexes [16,17]. This has been used on c-Si cells [6,14,17], CdTe [18], GaAs [19], InGaP [20], CIGS [21], DSSC, OPV, PSC [6]. QDs used for the purposes of power conversion efficiency (PCE) improvements can include a variety of commonly used QDs for biological and chemical uses, such as: Si-QDs, CQDs, CdS, CdSe, CdTe, $CuInS_2$, CuS, PbS, PbSe, CdSe/ZnS, ZnS, InP, InAs, Ag_2S, Bi_2S_3, Sb_2S_3, $CuInS_2$/ZnS, [8,19,20,22–25]. Deposition techniques varied and were dependent on the host material. Simple techniques consisted of spin coating [26,27], dropcasting [28], inkjet printing [29], plasma-enhanced chemical vapour deposition (PECVD) [30,31], and spin-on-glass [32].

The focus of this paper is the use of silicon quantum dots (Si-QDs) for the increase the power conversion efficiency (PCE) of pc-Si solar cells by luminescent downshifting. Previous works that have employed Si-QDs to enhance the performance of Si solar cells are summarised in Table 1.

Table 1. Overview of Si-QDs used on Si solar cells and enhancements achieved by previous studies.

Cell Type	Average Size of Si-QDs (nm)	λ_{exc} (nm)	λ_{em} (nm)	Surface Coating Method	ΔIsc (%) Increase	ΔPCE (%) Increase	LDS Layer Thickness (nm)	Ref.
pc-Si (commercial)	~3	325	660	Spin-coating in IPA	~2.3%	3.7% (fresh coat) 1.3% (after 11 days) 1.5% (after 41 days)	~120	[27]
sc-Si (commercial)	6.4	300 400 500	680	Spin-coating, SOG (spin-on-glass)	~1.3%	0.4% (actual) 1.2% (modelled at 100% DSE)	130	[32]
pc-Si (commercial)	~3 [27]	370	773	Inkjet in mesitylene	N/A	2%	74	[29]
c-Si solar cell	2–10	N/A	3–4 nm: 795 6–8 nm: 865 9–10 nm: 905	Spin-coating	N/A	12%	50–300	[33]
a-Si	2.85	365	628	Spin-coating	11.42%	N/A	2–7	[34]
pc-Si (BP Solarex Si)	1	254 365	328 (at λ_{exc} = 254 nm) 410 (at λ_{exc} = 365 nm)	Dropcast in IPA	17% (at 254, 365 nm) 4% (at 550–650 nm)	~62% (at 254, 365 nm) <3% (at 550–650 nm)	1–3	[28]
	2.85		630 (at λ_{exc} = 254, 365 nm)		5% (at 254, 365 nm) <5% (at 550–650 nm)	~67% (at 254 nm) 7.5–13.5% (at 550–650 nm)		

These reported increases in the short circuit current (Isc) of c-Si solar cells in the range of 1.3% to 4%. A high increase in the Isc of 17% under UV light and 4% under visible light in the range of 550–650 nm was reported with the use of Si-QDs of 1 nm size by Stupca et al. (2007), while a power increase between 7.5–13.5% in the aforementioned visible range was reported which was dominated by a substantial increase in the open circuit voltage (V_{oc}) [28]. A reduction in surface reflectance was reported as a factor in increasing the Isc of Si solar cells, observed in wavelength ranges of 300–500 nm and 640–1100 nm achieved through the use of Si-QDs [29], with reductions up to 4% [33].

The current study follows from previous works of one of the authors in [35–37] on phenylacetylene-capped silicon quantum dots (PA Si-QDs) and explores their potential application in pc-Si solar cells for performance enhancement through luminescent downshifting.

The specific use and novelty of PA Si-QDs for LDS applications rely on the properties of these QDs, which can be produced in substantial quantities using bottom-up methods mentioned in Section 2. Another benefit is the stable thermal diffusivity of these QDs which can help in stabilising solar cells thermally in addition to its LDS effects [35]. To the authors' knowledge, there is so far no study in the literature addressing the use of PA Si-QDs as an LDS layer. The paper emphasises the usefulness of the LDS properties of the PA Si-QDs in enhancing the Isc of pc-Si solar cells.

2. Experimental Procedure

2.1. Preparation of PA Si-QDs

The PA-capped Si-QDs were synthesised according to the methods reported in [35–37]. An amount of 1 g sodium (Na) and 4.2 g naphthalene were sonicated in 70 mL tetrahydrofuran (THF) for 2 h. This was then added to a dispersion of 1 mL silicon chloride in 200 mL tetrahydrofuran resulting in a brown suspension. To that is added a previously stirred (30 min) 20 mL THF solution of 2 mL PA, and 4.8 mL of n-butyllithium which was added to the THF/PA solution carefully by small drops. The PA/n-butyllithium THF solution was then carefully added to the Na/naphthalene THF solution and left to reflux for 8 h at a suitable temperature. The mixture was then washed using Di-water and diethyl ether; the solution was added to a separating funnel and allowed to rest for separation. This was repeated several times. The diethyl ether part was then reduced and dried on a rotavapor at 50 °C until a dry orange/brown powder was formed. The product is PA-capped Si-QDs. The reported mean diameter is 6 nm, with a standard deviation of 1 nm [37]. The FT-IR, TEM, NMR, and XPS measurements of the PA Si-QDs are provided in previous studies by one of the authors in [35–37].

2.2. Sample Preparation

In this study, 39 mm × 39 mm commercial pc-Si solar cells were used and characterised before and after deposition of the PA Si-QDs which was performed by dropcasting. Sample Q1 was prepared by dropcasting 0.15 mg of PA Si-QDs dissolved in 1 mL Dichloromethane (DCM) volatile and fast-drying solvent, while sample Q2 was prepared by dropcasting 0.01 mg of PA Si-QDs dissolved in 1 mL DCM. The DCM completely evaporates in less than 5 min leaving a uniform layer; the samples were kept on a flat surface to ensure no skewness is present.

2.3. Electrical and Optical Characterisation

The samples were characterised before and after freshly coated with PA Si-QDs. I-V characterisation was performed using ABET Technologies' model 11002 SunLite Solar Simulator (USA) and KEITHLEY Tektronix 2450 SourceMeter (UK) with the sample on a temperature-controlled vacuum chuck, under standard test conditions (STC); 1000 W/m^2 simulated solar irradiance at AM1.5, cell temperature 25 °C. A blue bandpass filter SCHOTT BG42 was also used in some of the experiments to examine performance mainly in the blue-green region.

Three control samples without any coating, used for reference purposes, R1, R2, and R3 were also characterised. The samples were also encapsulated using ethylene-vinyl acetate (EVA) film, a 3.2 mm Pilkington Optiwhite [38] low-iron extra clear float glass on top, and Tedlar backsheet. The encapsulation was carried out with the use of a hot air gun at 180 °C. The total device dimensions measured 50 mm × 50 mm.

Optical measurements involved diffuse and specular reflectance, using Ocean HDX Spectrometer with optical fibre and Halogen Light Source HL-2000-FHSA, diffuse and specular reflectance standards. Liquid sample fluorescence measurement was carried out using Edinburgh Instruments' FS5 Spectrofluorometer; PA Si-QDs dissolved in DCM. Fluorescence microscopy was carried out using ZEISS Axio Scope.A1 at 10× zoom, using Excelitas Technologies' X-Cite 120Q spectral excitation light source with multiple peaks at 335, 370, 410, 440, 550, and 580 nm.

3. Results and Analysis

3.1. Optical Measurements

Photoluminescence (PL) readings measured on an FS5 spectrofluorometer for a liquid sample of PA Si-QDs dissolved in host DCM are shown in Figure 1. The main two peaks shown are at 447 nm and 506 nm, where the sample was excited at 365 nm. The fluorescence microscopy of the coated sample is presented in Figure 2, showing the expected PL of the PA Si-QDs with cyan 506 nm colour in agreement with the measured PL readings of the liquid sample. The sample was excited with X-Cite 120 Q spectral excitation light source from 300–740 nm with peaks at 335, 370, 410, 440, 550, and 580 nm.

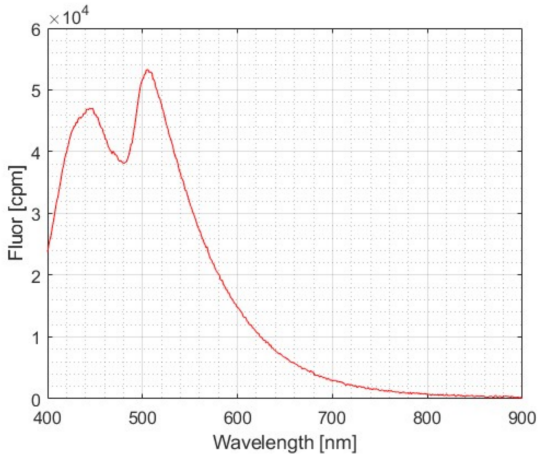

Figure 1. PL spectrum of liquid PA Si-QDs dissolved in DCM measured on FS5 spectrofluorometer.

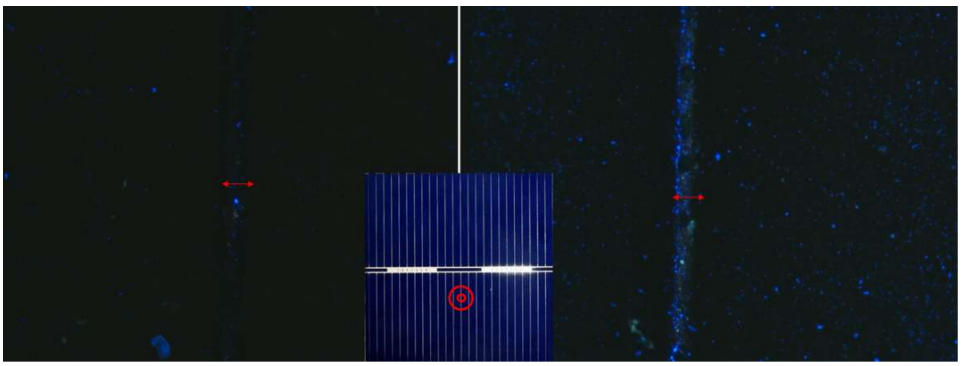

Figure 2. Fluorescence microscopy of two poly-Si solar cells; on the left, the fluorescence image of the bare cell, and on the right the fluorescence image of the coated sample with PA Si-QDs; in the middle is the image of the bare pc-Si solar cell the double circles pointing to the region of ×10 fluorescence microscopy. The arrows indicate the position of a silver finger.

Due to the nature of bottom-up chemical synthesis of these PA Si-QDs, the resulting product varies in size. The reported size range is 3–8 nm with an average size of 6 nm, [37]. The introduction of PA ligand as a form of passivation to the Si-QDs introduces indirect bandgaps that can alter the expected photoluminescence wavelength, thus shifting to shorter wavelengths [39].

The diffuse and specular reflectance of a bare and coated pc-Si cell with PA Si-QDs, sample Q2, is shown in Figure 3. The PA Si-QD coating led to a reduction in reflectance in the wavelength ranges between 340–480 nm and 700–920 nm with a small only increase in the range between 500–700 nm. Specifically, a reduction of up to 61.8% in specular reflectance is observed at 377 nm, and of 44.4% in diffuse reflectance at the same wavelength. Antireflection properties can be explained by the porosity of the PA Si-QDs films as they get deposited and dried onto the surface of the solar cell. It has been reported in the

literature a dominant decrease in reflectance of 18.75% between 300–400 nm when using Si-QDs on pc-Si solar cells [29]. Similarly, it was also reported that a reduction of 8.5% in reflectance was observed at 360–370 nm [34]. The observed reflectance agrees with the reported literature. Dealing with pc-Si solar cells which naturally possess a V-shaped rough surface, it was reported in the literature, that the removal/reduction of the Vs on the surface of a pc-Si cell reduces the reflection of the cells [40]. This can be possible reasoning as to why the deposition of PA Si-QDs caused a noticeable reduction in reflection.

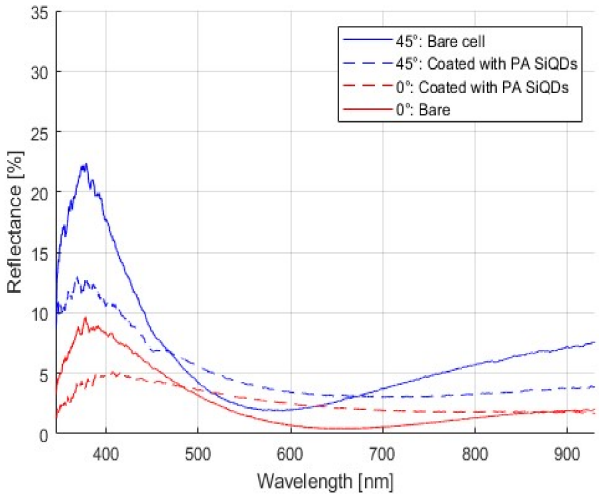

Figure 3. Diffuse and specular reflectance measured at 45° and 0°, respectively, for the bare and PA Si-QD coated pc-Si solar cell sample Q2.

3.2. Electrical Characterisation

The electrical parameters extracted from the I-V characteristics for the two samples Q1 and Q2 before and after the deposition of PA Si-QDs are displayed in Table 2. Both samples showed an increase in the Isc of 0.75% for Q1 and 1.06% for the Q2 sample. There is a negligible effect of the coating on Voc in Q1. The Voc in Q2, although slightly increased, lies within the range of the standard deviation as discussed in Section 4. The increase in Pm for the Q2 sample of 0.51% is attributed to the increase in the current. The I-V characteristics for the Q1 and Q2 samples before and after coating are displayed in Figure 4.

Table 2. Electrical parameters of samples Q1 and Q2 before and after coating with PA Si-QDs.

Samples	Electrical Parameters	Bare Solar Cell	Coated with PA Si-QDs	% Increase
Q1	Isc (A)	0.531	0.535	0.75
	Pm (W)	0.224	0.224	0.00
	Voc (V)	0.603	0.603	0.00
Q2	Isc (A)	0.472	0.477	1.06
	Pm (W)	0.193	0.194	0.51
	Voc (V)	0.582	0.583	0.17

The coated Q2 sample was further encapsulated with EVA within the glass on top and the Tedlar backsheet and its electrical characteristics before (bare cell) and after coating and encapsulation are shown in Table 3. A significant increase in the Isc of 11.86% and the Pm of 11.39% is observed mainly attributed to the increase in the current and the effect of encapsulation. The I-V characteristic of the bare and encapsulated sample is shown in Figure 5.

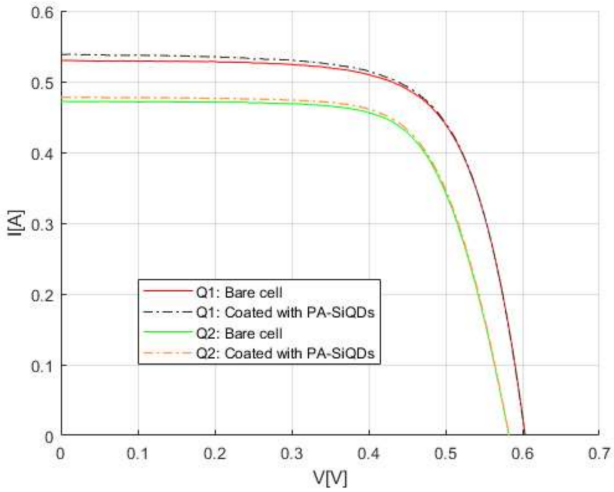

Figure 4. I-V characteristic of Q1 and Q2 samples before (bare cell) and after coated with PA Si-QDs.

Table 3. Electrical parameters of Q2 sample before coating (bare cell) and after coating with PA Si-QDs and encapsulation.

Electrical Parameters	Q2 Bare Sample	Q2 Coated and Encapsulated	% Increase
Isc (A)	0.472	0.528	11.86
Pm (W)	0.193	0.215	11.39
Voc (V)	0.582	0.586	0.69

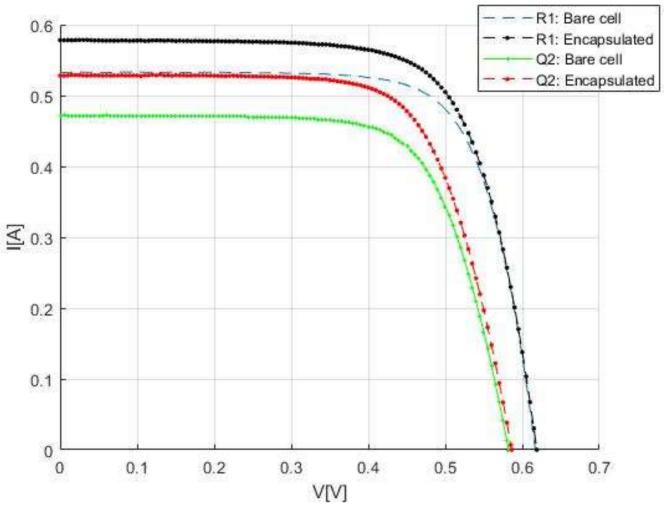

Figure 5. I-V characteristic of coated Q2 sample (with PA Si-QDs) and reference R1 sample before (bare cell) and after encapsulation.

To investigate the effect of encapsulation three separate solar cell samples used as reference were characterised before and after encapsulation. The results of the electrical parameters are shown in Table 4. The encapsulation led to an increase between 8.26–8.58% in the Isc; the large increase is due to the combination of internal back reflections at the interface with the glass and its high optical characteristics, and a similar increase of up to 8.7% in Pm. The I-V characteristic of the R1 sample is shown in Figure 5. In comparison, the Q2 sample coated with PA Si-QDs and encapsulated exhibits about 3.4% higher increase in the Isc and about 4.1% in the Pm compared to the increase in performance observed with encapsulation in the reference samples. This includes the 1% increase in the Isc due to the

PA Si-QD coating, while the rest is further enhancement due to the optical coupling as a result of the encapsulation.

Table 4. Electrical parameters of three reference samples before and after encapsulation.

Reference Cell Sample	Electrical Parameters	Average Values		% Increase
		Bare cell	Encapsulated	
R1	Isc (A)	0.533	0.577	8.26
	Pm (W)	0.240	0.253	5.42
	Voc (V)	0.616	0.619	0.49
R2	Isc (A)	0.548	0.595	8.58
	Pm (W)	0.229	0.249	8.73
	Voc (V)	0.612	0.614	0.33
R3	Isc (A)	0.543	0.589	8.47
	Pm (W)	0.243	0.262	7.81
	Voc (V)	0.620	0.622	0.32

In a further experiment, the incident simulated solar light was passed through a band-pass filter SCHOTT BG42, to examine the performance mainly in the blue-green region. The increase in the Isc for the encapsulated Q2 sample coated with PA Si-QDs reached 13.68% in comparison to the performance of the bare cell, as shown in Table 5, which may be explained by the higher internal back reflection at the interface with the glass which is more pronounced at these wavelengths. For comparison, the corresponding increase for the reference R1 encapsulated sample reached 11.57% in the blue-green region. The higher performance of the reference cell in this region compared to that under the unfiltered simulated solar light is attributed to the effect of encapsulation with higher internal reflections at blue wavelengths. The I-V characteristics for the bare and encapsulated coated Q2 sample and reference R1 sample for simulated solar light passing through the blue filter are presented in Figure 6.

Table 5. Electrical parameters of Q2 sample before coating (bare cell) and after coating and encapsulation, compared to reference sample R1 before and after encapsulation. The incident simulated solar light was reduced by a blue filter SCHOTT BG42.

Sample	Electrical Parameters	Bare Cell	Encapsulated Cell	% Increase
Q2	Isc (A)	0.117	0.133	13.68
	Pm (W)	0.044	0.051	15.91
	Voc (V)	0.524	0.527	0.57
R1	Isc (A)	0.121	0.135	11.57
	Pm (W)	0.051	0.055	7.84
	Voc (V)	0.574	0.570	−0.70

The difference in the increase in Isc between the coated samples is due to the reduction in the porosity of the PA Si-QDs films created. It was reported by Pi et al. (2012) that the increase in thickness of Si-QDs film from 16 nm to 74 nm has decreased the porosity from 84% to 69% [29]. The estimated thicknesses of deposited layers on the Q2 sample (0.01 mg) and the Q1 sample (0.15 mg) are 2.02 nm and 30.27 nm, respectively. This correlates with an increased reflectance and shading, thus a reduction in expected improvement by depositing higher thickness layers of PA Si-QDs on pc-Si solar cells. The layer thickness was estimated based on the uniformly deposited mass of PA Si-QDs times the density of PA and Si over the solar cell area.

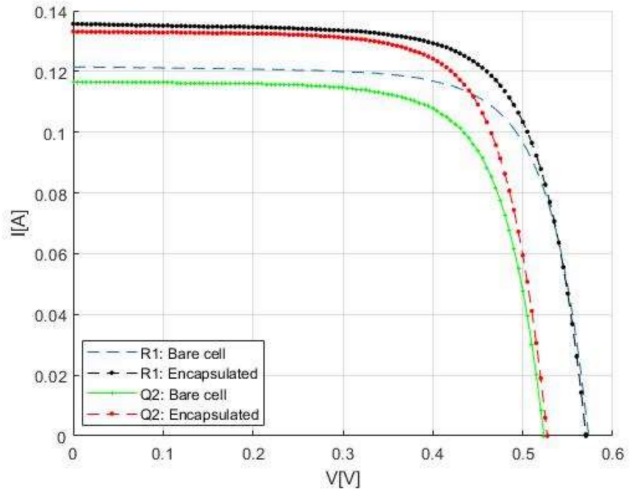

Figure 6. I-V characteristic for coated Q2 sample (with PA Si-QDs) and reference R1 sample with incident simulated solar light passing through a blue bandpass filter. The before coating (bare cell) and after encapsulation (and coating for Q2) curves are displayed.

The experimental results obtained for the increase In Isc, 1.06% for sample Q2 and 0.75% for sample Q1, are in agreement with similar increases reported in the literature of 1.3% [32] and 2.3% [27] in Isc for the use of Si-QDs to enhance the PCE of Si solar cells.

The significant increase in the performance of the encapsulated pc-Si solar cell may be attributed primarily to the improved optical combination that occurs as a result of eliminating air gaps and increased internal reflections. Mohan et al. (2020) have tested the improvements in encapsulation introduced to Si solar cells; interpreted from the graphs, it was shown that a drop of 55.5% in reflectance was observed at 300 nm. It was also shown that EQE was improved by 14.5% from 300 nm to 1000 nm [40].

4. Degradation and Reproducibility

A follow-up I-V characterisation of the encapsulated sample Q2 has been carried out 74 and 91 days after the first measurement to check on the stability of the sample over time, as shown in Figure 7.

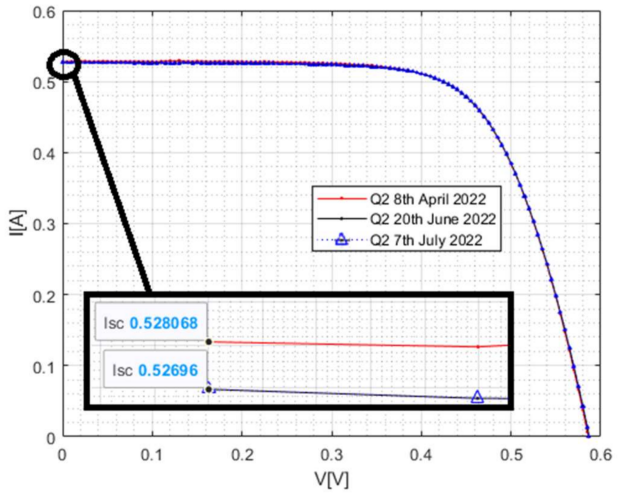

Figure 7. I-V characteristic for encapsulated and PA Si-QDs coated Q2 sample carried 74- and 91-days post encapsulation (overlapping).

A small drop in the Isc of the encapsulated Q2 sample was recorded 74 and 91 days after the initial characterisation of the fresh sample. The electrical parameter values shown

in Table 6 are average values of the measurements repeated three times. The standard deviation of the measurements is further shown in Table 7. While the accuracy of the I, V measurement with the KEITHLEY SMU lies in the fourth decimal place, the overall accuracy of the measurement considering the temporal stability of the light source (Class ABA), positioning, temperature control, and controlled environmental conditions, lies in the third decimal place, as shown in Table 7 with standard deviation 0.002. The values of Isc, Voc, and Pm shown in Table 6, corresponding to the three dates, do not differ essentially and lie within the standard deviation error domain, as shown in Table 7, which indicates that any reduction in performance is negligible and that the encapsulated sample has not essentially degraded within the period of 3 months. On the contrary, considering the standard deviation values for the original measurement of sample Q2, it is clear that the increase in performance is significant and outside the uncertainty range, and so the finding is secure.

Table 6. Electrical parameters of encapsulated and PA Si-QDs coated Q2 sample from characterisation carried out 74 and 91 days apart.

Electrical Parameters	8 April 2022	74 Days: 20 June 2022	% Increase	91 Days: 7 July 2022	% Increase
Isc (A)	0.528	0.527	−0.19	0.527	−0.19
Pm (W)	0.215	0.215	0.00	0.214	−0.47
Voc (V)	0.586	0.587	0.17	0.585	−0.17

Table 7. Standard deviation (STD) of Isc, Pm, and Voc for Q2 sample after coating with PA Si-QDs and encapsulation.

Date	8 April 2022	74 Days: 20 June 2022	91 Days: 7 July 2022
STD of Isc (A)	0.002	0.003	0.002
STD of Pm (W)	0.002	0.003	0.002
STD of Voc (V)	0.002	0.002	0.002

The minimal drop in the Isc after 74 and 91 days showcases the importance of encapsulation when using air-sensitive QDs such as the PA SiQDs as isolation from air preserves the LDS sample. On the other hand, the timed exposure to air between deposition and encapsulation may initiate an oxidation process that is only measurable months after the initial measurements. Further work is needed to study the effects of the degradation of the PA Si-QDs, which can be carried out by a TGA (thermogravimetric analysis) analysis, which can be modified to quantify oxidation.

To further test the reproducibility of the results, a new sample Q3 has been created, similarly to Q2, 85 days later, dropcasted with 0.01 mg of the PA Si-QD initially fabricated. The I-V characteristic for sample Q3 before and after being coated with PA Si-QDs is shown in Figure 8 and the electrical parameters extracted are shown in Table 8.

Table 8. Electrical parameters of Q3 sample before coating (bare cell) and after coating with PA Si-QDs 85 days later.

Electrical Parameters	Q3 Bare Sample	Q3 Coated with PA Si-QDs 85 Days Later	% Increase
Isc (A)	0.509	0.512	0.59
Pm (W)	0.212	0.211	−0.47
Voc (V)	0.602	0.600	−0.33

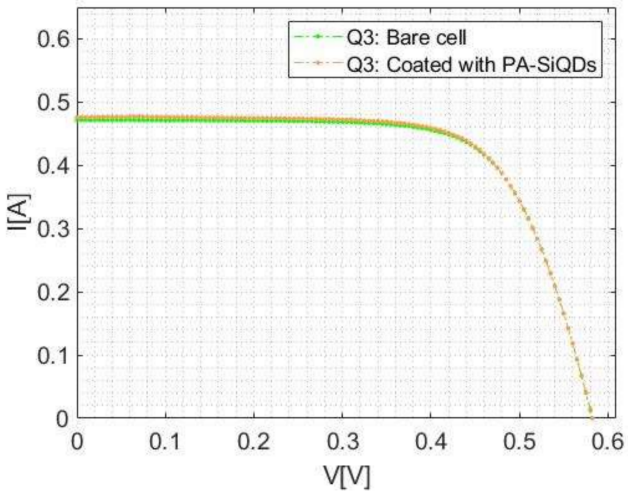

Figure 8. I-V characteristic Q3 sample before (bare cell) and after coated with PA Si-QDs.

The dropcasting of PA Si-QDs onto sample Q3, 85 days later, led to an increase of 0.59% in the Isc. The smaller increase of 0.59% in the Isc of sample Q3 compared to the 1.06% for sample Q2 indicates a degradation of the fabricated sample of PA Si-QDs. This suggests the importance of fresh deposition and encapsulation of the sample. On the other hand, the increase in the Isc in sample Q3 is a good representation of the reproducibility of the use of PA Si-QDs to enhance the performance of pc-Si solar cells.

5. Discussion

The significant drop in reflection at 377 nm (Figure 3) may be partly due to Rayleigh Scattering which is maximised in the UV range, especially if the QDs are smaller than 1/10 of the incident wavelength [41]; 37.7 nm in this case, where the average reported size of the PA Si-QDs is 6 nm [37], thus acting as an antireflective layer.

A blue bandpass filter, SCHOTT BG42, was used for an extra set of I-V characterisation. Its transmittance is 40% at 350 nm, and 65% at 405 nm, this renders a transmittance of less than 60% for 377 nm. It maximises at 514 nm with transmittance reaching 88% [42]. Table 9 shows the Isc for the Q2 sample before and after coating with PA Si-QDs when the incident light was passed through the bandpass filter. The standard deviation of the measurements in this case, under filtered light, is much smaller than that under the full simulated solar light and lies in the fourth decimal place, as shown in Table 9. The relative increase in the Isc after coating with PA Si-QDs is 1.2% with uncertainty estimated at $\pm$0.4%.

Table 9. Electrical parameters of Q2 sample before coating (bare cell) and after coating with PA Si-QDs. The incident simulated solar light was reduced by a blue bandpass filter SCHOTT BG42.

Sample	Electrical Parameters	Bare Cell	Coated with PA Si-QDs	% Increase
Q2	Isc (A)	0.1168	0.1182	1.2
	STD of Isc (A)	0.0001	0.0005	

As the filter blocks >40% of the light at wavelength 377 nm and 18% at the highest permissible wavelength of 514 nm, it would be expected that the increase in the Isc would drop significantly below 1.06%, which was at the full solar light exposure. Nevertheless, an increase of 1.2% in the Isc is measured, which further proves the LDS behaviour of the PA Si-QDs, where UV and near-UV light is downshifted to higher wavelengths.

pc-Si solar cells possess low EQEs in the UV region of the solar spectrum; with EQE dropping below 60% [43,44]. The low spectral response in the region below 400 nm indicates that the reduction in reflectance around 377 nm cannot be of much benefit to the solar

cell itself thus a measurable increase in the Isc due to antireflection alone may not be well supported to defend that the phenomenon is due to backscattering only. This indicates that the downshifting effects carried out by the PA Si-QDs are associated with the reduction in the reflection at 377 nm. With EQEs passing 90% past the 400 nm mark, downshifting to 447 nm and 506 nm is the main reason for the increase in the Isc.

6. Conclusions

This study outlined the use of PA Si-QDs as a downshifting material for the increase in the performance of pc-Si solar cells. The increase in the performance of the cells is explained by the LDS properties of the PA Si-QDs with photoluminescence at 447 nm and 506 nm when excited at 365 nm, as well as their anti-reflective properties as shown by the reduction in reflectance, measured at 61.8% in specular reflectance and 44.4% in diffuse reflectance at 377 nm.

The I-V characterisation of the Q1 (0.15 mg PA Si-QD) and Q2 (0.01 mg PA Si-QD) samples before and after coating with PA Si-QDs showed an average increase in Isc by 0.75% and 1.06%, respectively. Further increase in performance was observed for the fully encapsulated sample reaching a total increase in Isc higher by 3.4% and in Pm higher by 4.1% when compared to the increase in performance observed with encapsulation in the reference samples. This shows that the effect of optical coupling with encapsulation of the sample in the case of coated PA Si-QD solar cells increased the Isc further by about 2.2%.

The benefit of using PA Si-QDs as an LDS material over other Si-QDs and QDs in the literature resides in the capping ligand PA (phenylacetylene), it allows the core Si to have properties similar to that of bulk Si, yet have higher electrical conductivity compared to Si-QDs due to the overlap of these ligands as shown in [36,37]. One more benefit of capped Si-QDs is the prolonged shelf life compared to non-capped Si-QDs due to lower rates of oxidation as the valence electrons are occupied by the capping material. Overall, the preparation of PA Si-QD samples is straight forward and there is potential, as shown in this study, in their use for increasing the performance of pc-Si solar cells.

Author Contributions: Conceptualisation, E.K. and Y.C.; methodology, E.K and Y.C.; software, Q.M.; validation, Q.M., E.K. and Y.C.; formal analysis, E.K. and Q.M.; investigation, Q.M.; resources, Y.C. and E.K.; data curation, Q.M.; writing—original draft preparation, Q.M. and E.K.; writing—review and editing, Q.M., E.K. and Y.C.; visualisation, Q.M. and E.K.; supervision, E.K. and Y.C. All authors have read and agreed to the published version of the manuscript.

Funding: This research project is part of PhD work of QM which is funded by the Science Faculty of the University of East Anglia.

Data Availability Statement: The data presented in this study are available on request.

Acknowledgments: This project is part of PhD work of QM funded by the Science Faculty of the University of East Anglia which is much appreciated.

Conflicts of Interest: The authors declare no conflict of interest.

References

1. NREL. Best Research-Cell Efficiency Chart. Photovoltaic Research. 2021. Available online: https://www.nrel.gov/pv/cell-efficiency.html (accessed on 10 September 2021).
2. Green, M.A.; Emery, K.; Hishikawa, Y.; Warta, W.; Dunlop, E.D. Solar cell efficiency tables (version 48). *Prog. Photovolt. Res. Appl.* **2016**, *24*, 905–913. [CrossRef]
3. Green, M.; Dunlop, E.; Hohl-Ebinger, J.; Yoshita, M.; Kopidakis, N.; Hao, X. Solar cell efficiency tables (version 57). *Prog. Photovolt. Res. Appl.* **2021**, *29*, 3–15. [CrossRef]
4. Wirth, H. Crystalline Silicon PV Module Technology. In *Semiconductors and Semimetals*; Elsevier: Amsterdam, The Netherlands, 2013; Volume 89, pp. 135–197.
5. Nunzi, J.M. Requirements for a rectifying antenna solar cell technology. *Nanophotonics III* **2010**, *7712*, 771204.
6. McKenna, B.; Evans, R.C. Towards Efficient Spectral Converters through Materials Design for Luminescent Solar Devices. *Adv. Mater.* **2017**, *29*, 1–23. [CrossRef] [PubMed]
7. Dexter, D.L. Possibility of luminescent quantum yields greater than unity. *Phys. Rev.* **1957**, *108*, 630–633. [CrossRef]

8. De la Mora, M.B.; Amelines-Sarria, O.; Monroy, B.M.; Hernández-Pérez, C.D.; Lugo, J.E. Materials for downconversion in solar cells: Perspectives and challenges. *Sol. Energy Mater. Sol. Cells* **2017**, *165*, 59–71. [CrossRef]
9. Bünzli, J.C.G.; Chauvin, A.S. Lanthanides in Solar Energy Conversion. *Handb. Phys. Chem. Rare Earths* **2014**, *44*, 169–281.
10. Bartram, R.H.; Lempicki, A. Electron multiplication in scintillators and phosphors. *J. Lumin.* **1997**, *72–74*, 734–736. [CrossRef]
11. Ronda, C. Luminescent materials with quantum efficiency larger than 1, status and prospects. *J. Lumin.* **2002**, *100*, 301–305. [CrossRef]
12. Richards, B.S. Luminescent layers for enhanced silicon solar cell performance: Down-conversion. *Sol. Energy Mater. Sol. Cells* **2006**, *90*, 1189–1207. [CrossRef]
13. Shalav, A.; Richards, B.S.; Green, M.A. Luminescent layers for enhanced silicon solar cell performance: Up-conversion. *Sol. Energy Mater. Sol. Cells* **2007**, *91*, 829–842. [CrossRef]
14. Ahmed, H.; McCormack, S.J.; Doran, J. External Quantum Efficiency Improvement with Luminescent Downshifting Layers: Experimental and Modelling. 2016. Available online: https://downloads.hindawi.com/archive/2016/8543475.pdf (accessed on 22 April 2022).
15. Hovel, H.J.; Hodgson, R.T.; Woodall, J.M. The effect of fluorescent wavelength shifting on solar cell spectral response. *Sol. Energy Mater.* **1979**, *2*, 19–29. [CrossRef]
16. Klampaftis, E.; Ross, D.; McIntosh, K.R.; Richards, B.S. Enhancing the performance of solar cells via luminescent down-shifting of the incident spectrum: A review. *Sol. Energy Mater. Sol. Cells* **2009**, *93*, 1182–1194. [CrossRef]
17. Alonso-Álvarez, D.; Ross, D.; Klampaftis, E.; McIntosh, K.R.; Jia, S.; Storiz, P.; Stolz, T.; Richards, B.S. Luminescent down-shifting experiment and modelling with multiple photovoltaic technologies. *Prog. Photovolt. Res. Appl.* **2015**, *23*, 479–497. [CrossRef]
18. Van Der Ende, B.M.; Aarts, L.; Meijerink, A. Lanthanide ions as spectral converters for solar cells. *Phys. Chem. Chem. Phys.* **2009**, *11*, 11081–11095. [CrossRef] [PubMed]
19. Han, H.V.; Lin, C.C.; Tsai, Y.L.; Chen, H.C.; Chen, K.J.; Yeh, Y.L.; Lin, W.Y.; Kuo, H.C.; Yu, P. A Highly Efficient Hybrid GaAs Solar Cell Based on Colloidal-Quantum-Dot-Sensitization. *Sci. Rep.* **2014**, *4*, 5734. [CrossRef]
20. Krishnan, C.; Mercier, T.; Rahman, T.; Piana, G.; Brossard, M.; Yagafarov, T.; To, A.; Pollard, M.E.; Shaw, P.; Bagnall, D.M.; et al. Efficient light harvesting in hybrid quantum dot-interdigitated back contact solar cells: Via resonant energy transfer and luminescent downshifting. *Nanoscale* **2019**, *11*, 18837–18844. [CrossRef]
21. Solodovnyk, A.; Kick, C.; Osvet, A.; Egelhaaf, H.J.; Stern, E.; Batentschuk, M.; Forberich, K.; Brabec, C.J. Optimization of Solution-Processed Luminescent Down-Shifting Layers for Photovoltaics by Customizing Organic Dye Based Thick Films. *Energy Technol.* **2016**, *4*, 385–392. [CrossRef]
22. Gardelis, S.; Nassiopoulou, A.G. Evidence of significant down-conversion in a Si-based solar cell using $CuInS_2$/ZnS core shell quantum dots. *Appl. Phys. Lett.* **2014**, *104*, 183902. [CrossRef]
23. Nakamura, Y.; Iso, Y.; Isobe, T. Bandgap-Tuned $CuInS_2$/ZnS Core/Shell Quantum Dots for a Luminescent Downshifting Layer in a Crystalline Silicon Solar Module. *ACS Appl. Nano Mater.* **2020**, *3*, 3417–3426. [CrossRef]
24. Etgar, L. Semiconductor Nanocrystals as Light Harvesters in Solar Cells. *Materials* **2013**, *6*, 445–459. [CrossRef] [PubMed]
25. Liu, X.; Shan, D.; Ji, Y.; Li, D.; Li, W.; Xua, J.; Chen, K. Improved device performance of Si-based heterojunction solar cells by using phosphorus doped Si nanocrystals embedded in SiC host matrix. *AIP Adv.* **2019**, *9*, 025213. [CrossRef]
26. Kumar, K.; Subramanian, H. Spin coating of Silver Nanoparticles and Silicon Quantum Dots for Enhanced Down Conversion Efficiency. Master's Thesis, Delft University of Technology, Delft, The Netherlands, December 2013.
27. Pi, X.; Li, Q.; Li, D.; Yang, D. Spin-coating silicon-quantum-dot ink to improve solar cell efficiency. *Sol. Energy Mater. Sol. Cells* **2011**, *95*, 2941–2945. [CrossRef]
28. Stupca, M.; Alsalhi, M.; Al Saud, T.; Almuhanna, A.; Nayfeh, M.H. Enhancement of polycrystalline silicon solar cells using ultrathin films of silicon nanoparticle. *Appl. Phys. Lett.* **2007**, *91*, 063107. [CrossRef]
29. Pi, X.; Zhang, L.; Yang, D. Enhancing the Efficiency of Multicrystalline Silicon Solar Cells by the Inkjet Printing of Silicon-Quantum-Dot Ink. 2012. Available online: https://pubs.acs.org/doi/10.1021/jp307078g (accessed on 1 July 2020).
30. Sacks, J.; Savidge, R.M.; Gabr, A.; Walker, A.; Beal, R.; Wheeldon, J.; Knights, A.P.; Mascher, P.; Hinzer, K.; Kleiman, R.N. Quantum efficiency measurements of down-shifting using silicon nanocrystals for photovoltaic applications. In Proceedings of the Conference Record of the IEEE Photovoltaic Specialists Conference, Austin, TX, USA, 3–8 June 2012; pp. 92–96.
31. Remolina, A.; Monroy, B.M.; Garcia-Sanchez, M.F.; Ponce, A. Polymorphous silicon thin films obtained by plasma-enhanced chemical vapor depositionusing dichlorosilane as silicon precursor. *Nanotechnology* **2009**, *20*, 245604. [CrossRef]
32. Švrček, V.; Slaoui, A.; Muller, J.C. Silicon nanocrystals as light converter for solar cells. *Thin Solid Film.* **2004**, *451–452*, 384–388. [CrossRef]
33. Gribov, B.G.; Zinov'ev, K.V.; Kalashnik, O.N.; Gerasimenko, N.N.; Smirnov, D.I.; Sukhanov, V.N.; Kononov, N.N.; Dorofeev, S.G. Production of Silicon Nanoparticles for Use in Solar Cells. *Semiconductors* **2018**, *51*, 1675–1680. [CrossRef]
34. Chowdhury, F.I.; Alnuaimi, A.; El-Atab, N.; Nayfeh, M.; Nayfeh, A. Enhanced performance of thin-film amorphous silicon solar cells with a top film of 2.85 nm silicon nanoparticles. *Sol. Energy* **2016**, *125*, 332–338. [CrossRef]
35. Ashby, S.P.; Bian, T.; Ning, H.; Reece, M.J.; Chao, Y. Thermal Diffusivity of SPS Pressed Silicon Powders and the Potential for Using Bottom-Up Silicon Quantum Dots as a Starting Material. 2014. Available online: https://link.springer.com/article/10.1007/s11664-014-3599-y (accessed on 30 January 2020).

36. Ashby, S.P.; García-Cañadas, J.; Min, G.; Chao, Y. Measurement of thermoelectric properties of phenylacetylene-capped silicon nanoparticles and their potential in fabrication of thermoelectric materials. *J. Electron. Mater.* **2013**, *42*, 1495–1498. [CrossRef]
37. Ashby, S.P. Thomas, J.A.; García-Cañadas, J.; Min, G.; Corps, J.; Powell, A.V.; Xu, H.; Shend, W.; Chao, Y. Bridging Silicon Nanoparticles and Thermoelectrics: Phenylacetylene Functionalization. *Faraday Discuss.* **2014**, *176*, 349–361. [CrossRef]
38. Pilkington. Pilkington Optiwhite^{TM} for Solar Applications. 2022. Available online: https://www.pilkington.com/en/global/products/product-categories/solar-energy/pilkington-optiwhite-for-solar-applications#productrange (accessed on 29 October 2021).
39. Krishnamurthy Grandhi, G.; Arunkumar, M.; Viswanatha, R. Understanding the Role of Surface Capping Ligands in Passivating the Quantum Dots Using Copper Dopants as Internal Sensor. *J. Phys. Chem.* **2016**, *120*, 19785–19795.
40. Nakaya, H.; Nishida, M.; Takeda, Y.; Moriuchi, S.; Tonegawa, T.; Machida, T.; Nunoi, T. Polycrystalline silicon solar cells with V-grooved surface. *Sol. Energy Mater. Sol. Cells* **1994**, *34*, 219–225. [CrossRef]
41. Mirin, R.P.; Gossard, A.C.; Bowers, J.E. Characterization of InGaAs quantum dot lasers with a single quantum dot layer as an active region. *Phys. E Low-Dimens. Syst. Nanostruct.* **1998**, *2*, 738–742. [CrossRef]
42. SCHOTT. Advanced Optics, "BG42". 2022. Available online: https://www.schott.com/shop/advanced-optics/en/Matt-Filter-Plates/BG42/c/glass-BG42 (accessed on 8 March 2022).
43. Khaleda, M.Z.F.; Vengadaesvaran, B.; Rahim, N.A. Spectral response and quantum efficiency evaluation of solar cells: A review. In *Energy Materials: Fundamentals to Applications*; Elsevier: Amsterdam, The Netherlands, 2021; pp. 525–566.
44. Van Sark, W.G.J.H.M.; Meijerink, A.; Schropp, R.E.I. *Solar Spectrum Conversion for Photovoltaics Using Nanoparticles*; IntechOpen: Rijeka, Croatia, 2012.